Article

Metal Ion-Induced Formation of Metallogels by Visible-Light-Responsive Phenylalanine-Functionalized Arylazopyrazole Ligands

Mikayla Browning, Alexandra Jefferson, Jazz Geter and Kesete Ghebreyessus *

Department of Chemistry and Biochemistry, Hampton University, Hampton, VA 23668, USA;
mikayla.browning@hamptonu.edu (M.B.); alexandra.jefferson@hamptonu.edu (A.J.); jazzgeter@gmail.com (J.G.)
* Correspondence: kesete.ghebreyessus@hamptonu.edu; Tel.: +1-757-727-5475

Abstract: A visible-light-responsive arylazopyrazole-functionalized phenylalanine (4-MeS-AAP-NF) derived ligand was designed and synthesized, and it was found to form metallogels with reversible photo-responsive properties in mixed methanol/water (MeOH/H_2O) solvents. The gelation behavior of the 4-MeS-AAP-NF ligand in the presence of different divalent metal ions in mixed methanol/water (MeOH/H_2O) solvents at pH~11.60 was studied. It was found that the 4-MeS-AAP-NF ligand alone could not self-assemble to form any gels. However, in the presence of divalent metal ions, it readily formed the assembled metallogels in an alkaline aqueous/methanol solution with various morphologies. The results suggest that the gelation process was triggered by divalent metal ions. The presence of the AAP moiety in the gel matrix rendered the metallogel assemblies photo-responsive, and the reversible gel-to-sol phase transition was studied by UV-vis spectroscopy. The gels showed a slow, reversible visible-light-induced gel-to-sol phase transition under blue ($\lambda = 405$ nm) and then sol-to-gel transition by green light ($\lambda = 530$ nm) irradiation, resulting in the re-formation of the original gel state. The morphology and viscoelastic properties of the yellow–orange opaque metallogels were characterized by scanning electron microscopy (SEM) and rheological measurement, respectively.

Keywords: photoswitchable ligand; arylazopyrazole; metallogels; trans-to-cis isomerization

check for updates

1. Introduction

The self-assembly of supramolecular gels from low molecular weight gelators (LMWGs) has been recognized as an attractive approach to generate an advanced class of soft nanoscale materials with numerous potential applications such as sensors, actuators, and drug delivery systems [1–10]. Owing to their unique properties, LMWGs based on amino acids and short peptides have proven to be excellent building blocks for constructing supramolecular gels [11–18]. They offer a wide range of structural diversity, self-assembly properties, and morphological variations due to their facile gelation ability and ease of modulation of the structural and functional properties by varying the different amino acid types and sequences. These small molecules self-assemble into supramolecular gels due to their ability to form fibrillar networks and construct polymeric structures through non-covalent interactions that include hydrogen bonding, π–π stacking, and hydrophobic interactions.

Supramolecular gels that can be formed with the assistance of metal ions also offer a promising platform for the fabrication of highly processable and multi-stimuli responsive metallogels [4,5,8,10,13–20]. These organic–inorganic hybrids and biohybrids are key for creating highly functional materials that integrate the physicochemical behavior of the metal ions in the gel matrix. The incorporation of metal components and the manipulation of the metal–ligand interaction provides an effective way to subtly tune gelation ability and morphology. It is well-known that different peptides or amino acids provide multiple binding sites and

form complexes with various metal ions that can promote gelation by the formation of cross-linked supramolecular assemblies [12–18]. Metals coordinated with amino acids exhibit attractive dynamic and self-healing properties through the integration of the interesting and unique properties of metal ions into gelator molecules [3,13]. Enabling these systems to become stimuli-responsive can allow for the controlled assembly/disassembly of systems or can induce geometry changes and trigger guest release, adding an additional layer of information [7,8,15,19–23]. In recent years, a variety of photo-responsive moieties have been incorporated into amino acids/peptides to design photo-responsive gelators which can display switchable, smart, and emerging features [15,19,21,24]. Notably, azobenzene derivatives have been extensively explored in constructing such kinds of gels, in which the reversible photoisomerization significantly influences the polarity of both isomers and their interactions with solvents, leading to a greater effect on the gelation ability/process [19,21,24]. Stimuli responsiveness of these soft gel materials with highly permeable network structures offers potential applications in drug delivery and other fields.

More recently, arylazopyrazole (AAP) derivatives have been introduced as improved light-responsive molecular switches compared to their azobenzene counterparts and serve as important photochromic building blocks to attain smart supramolecular gels [25–29]. Given their superior properties, AAPs have drawn significant attention for their potential applications in the development of several supramolecular systems ranging from host–guest complexes, foams, adhesives, DNA complexes, light-responsive peptide hydrogels with host–guest interactions, and coordination complexes [30–34]. However, the vast majority of AAP-based systems used in these materials use high-energy UV light. In comparison with UV light, visible light is more suitable for use with organic and biomaterials to prevent photodamage [28,29]. Visible-light-responsive molecular switches alleviate the detrimental effects of high-energy UV light and facilitate the application of light-driven materials for biological and biomedical purposes. Though there are several reports on the design and synthesis of new ligand systems with the potential to form metallogels in suitable solvents, the discovery and development of visible-light-responsive amino acid-based ligands will have potential applications in the creation of new bio-hybrid materials for nano and biotechnology applications.

In this study, we report the fabrication of a visible-light-responsive metallogel system assembled from a phenylalanine-substituted arylazopyrazole-based LMWG ligand (4-MeS-AAP-NF) in the presence of divalent metal ions in alkaline aqueous solution at pH~11.60 (Figure 1).
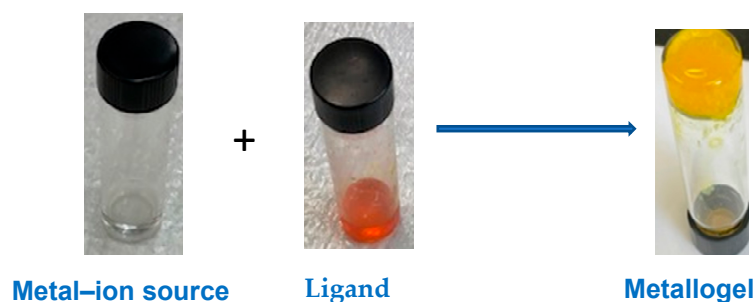

Metal–ion source   **Ligand**   **Metallogel**

Figure 1. Self-assembly of the divalent metal–ion triggered the formation of photo-responsive metallogels.

The formation of the stable gels was induced by the divalent metal ions under alkaline conditions facilitated through vortex or sonication treatment. The 4-MeS-AAP-NF, which possess multiple pendant groups of N-atoms and COO^- units, enables us to chelate metal ions and can serve as an excellent LMWG ligand to fabricate metallogels through the synergistic effects of metal–ion coordination and a variety of non-covalent secondary interactions such hydrogen bonding and π–π stacking interactions. The presence of the carboxylic acid and N-H functional groups in the 4-MeS-AAP-NF moiety allows them to

form a hydrogen-bonding interaction and provide a metal-coordinating site through the N-pyrazole ligand, which could facilitate the formation of stable gels. Furthermore, the phenylalanine moiety also possesses pH-responsive properties, which might provide the possibility to tune the self-assembly by adjusting the pH and further enhance gelation ability. Moreover, with the incorporation of the AAP photo-switchable azo moiety in the ligand structure, the metallogels can display light-induced sol–gel phase transitions.

2. Materials and Methods

2.1. General Information

All reactions were conducted under nitrogen. All chemicals and solvents were purchased from commercial sources and used as received. ^{1}H-NMR and ^{13}C-NMR spectra were recorded on a JEOL Eclipse2-400 MHz spectrometer (JEOL USA, Inc., Peabody, MA, USA), using solvent resonances as internal references. UV-vis spectra were recorded using a Carry 60-Bio series spectrometer from Agilent, (Agilent Technologies, Inc., Santa Clara, CA, USA). Fourier transform infrared spectra (FTIR) were collected on an attenuated total reflectance Fourier transform infrared (ATR-FTIR) spectrometer from Agilent equipped with a universal ATR sampling accessor. Spectra were obtained by collecting thirty-two scans with a resolution of 4 cm^{-1}. Scanning electron microscopy (SEM) studies were obtained using (SEMJEOL JSM-6060LV, JEOL USA, Inc.), operating with an accelerating voltage of 5–30 kV. The xerogels were prepared by drying in an oven at 70 °C overnight. To minimize charging, the samples were coated with a thin layer of gold before the experiment. Dynamic rheological measurements were conducted on an MCR 302 (Anton Paar) instrument (Anton Paar Inc., Ashaland, VA, USA). The hybrid gels were scooped, placed over the rheometer plate, and allowed to equilibrate for 15 min. Rheological experiments for all the gels were conducted at a temperature of 25 °C.

2.2. Spectroscopic Measurements

Dry acetonitrile, dimethyl sulfoxide (DMSO), and dichloromethane solvents were used for all UV-vis measurements. UV-vis absorption spectra were recorded on an Agilent Cary 60-BIO spectrometer (Agilent Technologies, Inc). Photoisomerization was induced by irradiating DMSO solutions of the precursor ligands and metallogles in a quartz cuvette at room temperature with blue (λ = 405 nm) and green (λ = 530 nm) light, followed by immediate recording of the absorption spectrum. The extent of isomerization at the photostationary state was estimated based on the following difference equation:

$$\% \, \text{Cis} = \frac{A_{trans} - A_{Cis}}{A_{trans}} \times 100$$

where A_{trans} is the absorbance of the *trans* isomer at λ$_{max}$ before light irradiation, and A_{cis} is the absorbance of the *cis* isomer at the same wavelength measured in the photostationary state [35–37].

2.3. Experimental Procedure

2.3.1. Synthesis of 2-(Methylthio)-3-(2-phenylhydrazono)pentane-2,4-dione (**2a**)

A solution of 2-(methylthio) aniline (1.49 g, 7.4 mmol) was prepared in acetic acid (CH$_3$CO$_2$H) (10 mL) and concentrated hydrochloric acid (Coc. HCl) (1.7 mL) in a round bottom flask. Then, a solution of sodium nitrite (NaNO$_2$) (0.610 g, 8.84 mmol) dissolved in H$_2$O (2.5 mL) at 0 °C was added dropwise [25]. The reaction mixture was allowed to stir for 1 h. Meanwhile, a solution of pentane-2,4-dione (0.98 mL, 9.8 mmol) and sodium acetate (NaCH$_3$CO$_2$) (1.81 g, 22.06 mmol) in ethanol (7 mL) and water (4 mL) was prepared. After 1 h, the reaction mixture containing the in situ-formed diazonium salt was transferred to the newly prepared solution of the pentan-2,4-dione. The mixture was stirred for another 1–3 h at room temperature. After completion of the reaction, the orange precipitate formed was separated by filtration and washed with ethanol and water (1:1), followed by hexane. The precipitate was kept under vacuum until complete dryness.

Orange solid; yield (1.7 g, 92%; **2a**). ^{1}H-NMR (400 MHz, CDCl$_3$), (δ ppm): δ: 14.80 (s, 1H), 7.36 (d, J = 7.8 Hz, 2H), 7.30 (d, J = 7.8 Hz, 2H), 2.60 (s, 3H), 2.50 (s, 3H), 2.48 (s, 3H). ^{13}C NMR (100 MHz, CDCl$_3$) (δ ppm): δ: 198.0, 197.1, 139.2, 136.2, 133.2, 128.1, 116.9, 31.8, 26.7, 16.4. Anal. Calcd for C$_{12}$H$_{14}$O$_2$N$_2$S: C, 57.58, H, 5.64, N, 11.19. Found: 57.37, H, 5.60, N, 10.80.

2.3.2. Synthesis of 2-(Methylthio)-3,5-dimethyl-(4-phenyldiazenyl)-1H-pyrazole (**3a**)

To a solution of 2-(methylthio)-3-(2-phenylhydrazono)pentane-2,4-dione (**2a**) (1.0 g, 4.0 mmol) in ethanol (50 mL), hydrazine hydrate (0.309 g, 6.0 mmol) was added, and the reaction mixture was allowed to reflux for 5 h in an oil bath. After completion of the reaction, the solvent was evaporated under reduced pressure, yielding 0.85 g of a yellow solid (86%).

Orange solid; yield (0.85 g, 86%; **3a**). ^{1}H-NMR (400 MHz, CDCl$_3$), (δ ppm): δ: 7.75 (m, 1H), 7.72 (m, 1H), 7.32 (m, 1H), 7.30 (s, 1H), 2.59 (s, 6H), 2.54 (s, 3H). ^{13}C NMR (100 MHz, CDCl$_3$) (δ ppm): δ: 150.9, 140.5, 134.60, 126.2 (2C), 122.2 (2C), 15.5 (2C), 12.1. Anal. Calcd. For C$_{12}$H$_{14}$N$_4$S: C, 58.51, H, 5.73, N, 22.74. Found: 58.30, H, 5.70, N, 22.43.

2.3.3. Synthesis of 2-(Methylthio)-3,5-dimethyl-(4-phenyldiazenyl)-N-CH$_2$CO$_2$CH$_2$CH$_3$ (**4a**)

To a solution of 2-(methylthio)-3,5-dimethyl-1H- pyrazole (**3a**) (0.904 g, 4.0 mmol) in dry acetonitrile (50 mL), potassium carbonate (K$_2$CO$_3$) (1.40 g, 3 eq) and ethyl chloroacetate (0.61 g,1.3 eq) were added and the reaction mixture was allowed to reflux for 24 h in an oil bath. After completion of the reaction, the solvent was evaporated under reduced pressure, affording the desired product (**4a**) as a yellow solid.

Yellow solid; yield (1.10 g, 83%; **4a**). ^{1}H NMR (400 MHz, CDCl$_3$) (ppm): 7.73 (d, J = 8.24 Hz, 2H), 7.31 (d, J = 8.24 Hz, 2H), 4.83 (s, 2H), 4.25 (q, J = 6.88 Hz, 2H), 2.55 (s, 3H), 2.53 (s, 3H), 2.50 (s, 3H), 1.29 (t, J = 7.36 Hz, 3H). ^{13}C NMR (100 MHz) (ppm): δ: 167.3, 151.0, 143.3, 140.5, 139.6, 135.4, 126.3, 122.3, 62.0, 50.6, 15.6, 14.1,14.0, 9.8. Anal. Calcd. for C$_{16}$H$_{20}$O$_2$N$_4$S: C, 57.81, H, 6.06, N, 16.85. Found: C, 57.52, H, 6.00, N, 16.55.

2.3.4. Synthesis of-2-(Methylthio)-3,5-dimethyl-(4-phenyldiazenyl)-N-CH$_2$CO$_2$H (**5a**)

The yellow precipitate (**4a**) was dissolved in ethanol (200 mL), and 1 M sodium hydroxide solution (25 mL) was added. The solution was then stirred for 24 h at room temperature. Then, the mixture was acidified by dropwise addition of 1M HCl solution to pH 3. The yellow precipitate formed was separated by filtration and air-dried.

Yellow solid; yield (1.0 g, 82%; **5a**). ^{1}H NMR (400 MHz, CDCl$_3$) (ppm): δ: 7.72 (m,1H) 7.36 (m, 1H) 7.30 (m, 1H), 7.17 (m, 1H), 4.88 (s, 2H), 2.59 (s, 3H), 2.49 (s, 3H), 2.46 (s, 3H). ^{13}C NMR (100 MHz) (ppm): δ: 168.7, 148.4, 141.5, 140.2, 139.0, 135.2, 129.7, 123.8, 123.7, 114.7, 50.2, 13.8, 13.6, 9.3. Anal. Calcd. for C$_{14}$H$_{16}$O$_2$N$_4$S: C, 55.25, H, 5.30, N, 18.41. Found: C, 55.05, H, 3.26, N, 18.01.

2.3.5. Synthesis of 2-(Methylthio)-3,5-dimethyl-(4-phenyldiazenyl)-N-methylenel-L-phenylalanine (4-MeS-AAP-NF; **6a**)

To a solution of 2-(Methylthio)-3,5-dimethyl-N-CH$_2$CO$_2$H (**5a**) (0.35g, 1.15 mmol) in chloroform (20 mL), N-hydroxysuccinimide (NHS) (0.133 g, 1.15 mmol) and N,N′-Dicyclohexyl-carbodiimide (DCC) (0.26 g, 1.15 mmol) were added. Then, the mixture was stirred for five hours at room temperature [38]. After completion of the reaction, the solvent was removed by rotary evaporation. The crude product was used without further purification for the next step of the reaction. This product was dissolved in 20 mL of acetone. To this solution, L-phenylalanine (0.235 g, 1.15 mmol) and sodium carbonate (0.488g, 4.60 mmol) dissolved in water (8 mL) were added, and the mixture was stirred overnight at room temperature. The solvent was removed by rotary evaporation, yielding a yellow solid. The crude product was then purified by silica gel column chromatography using dichloromethane/methanol solvent mixtures affording the desired photo-switchable phenylalanine conjugated 4-MeS-AAP-NF (**6a**).

Yellow solid; yield (0.42 g, 81%; **6a**). ^{1}H NMR (400 MHz, DMSO) (ppm): δ: 8.56 (d, J = 7.80 Hz, 1H, N-H), 7.69 (d, J = 8.24 Hz, 2H), 7.37 (d, J = 8.68 Hz, 2H), 7.31–7.22 (m, 5H), 4.76 (d, J = 7.76 Hz, 2H), 4.47 (m, 1H), 3.07–2.91 (m, 2H), 2.54 (s, 3H), 2.37 (s, 3H), 2.34 (s, 3H). ^{13}C NMR (100 MHz) (ppm): δ: 170.5, 165.2, 157.2, 152.3, 14.9, 141.5, 140.1, 139.8, 135.7, 130.7, 130.1, 128.1, 126.1, 124.9, 115.4, 52.5, 48.0, 33.9, 14.6, 14.1, 9.9. ESI-MS m/z calcd for $C_{23}H_{25}N_5O_3S$ [M + H]$^+$ 452.1751; found: 452.1750.
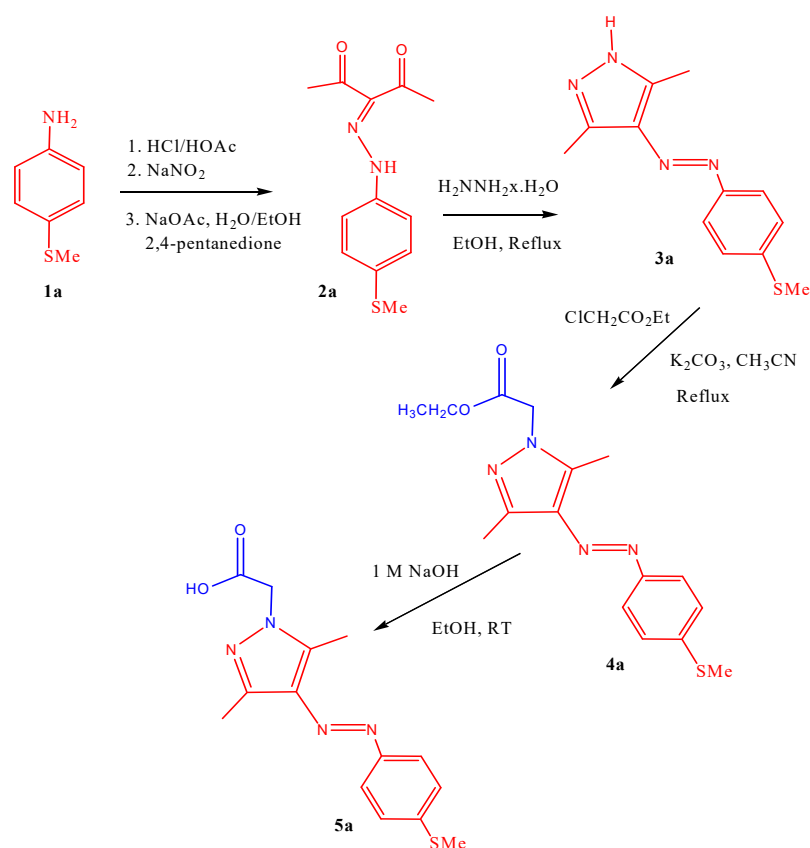
3. Results and Discussion

3.1. Synthesis and Characterization
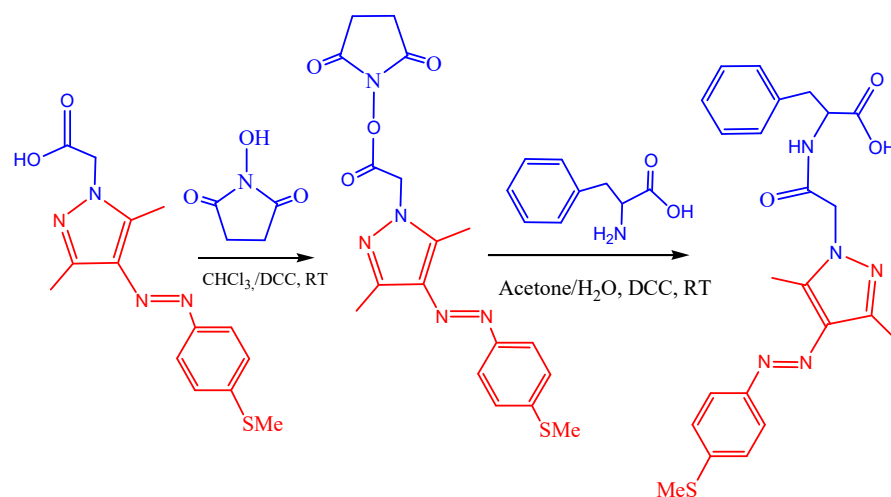
3.1.1. Synthesis of 4-MeS-AAP-CH$_2$CO$_2$H (**5a**)

Starting from the commercially available 4-thiomethyl-aniline derivative, the carboxylic acid-functionalized arylazopyrazole moiety, 4-MeS-AAP-CH$_2$CO$_2$H (**5a**), was synthesized in four simple steps (Scheme 1) following standard literature methods and procedures developed in our laboratory [15,25–29]. First, the 4-thiometyl-anline (**1a**) derivative was converted into a diazonium salt by hydrochloric acid and sodium nitrite, which was subsequently reacted in situ with 2,4-pentandione to afford the precursor hydrazone as a yellow solid in high yield (**2a**). Reaction of the resulting hydrazone with hydrazine. Xhydrate under reflux conditions afforded the corresponding intermediate compound (**3a**). Treatment of the resulting **3a** intermediate compound with ethyl chloroacetate in refluxing acetonitrile and in the presence of potassium carbonate as a base afforded the ester functionalized compound **4a**. Base hydrolysis of the resulting intermediate compound **4a** afforded the desired 4-MeS-AAP-CH$_2$CO$_2$H (**5a**) molecular switch in good yield. Details of the synthesis and analysis of all the 4-MeS-AAP-CH$_2$CO$_2$H (**5a**) are provided in the experimental section. The structural characterization of all the intermediate compounds and the final product was carried out using ^{1}H-NMR and ^{13}C-NMR spectroscopy. The NMR results confirm that molecular switches exist in their more stable trans-isomers under normal conditions. This was confirmed by the characteristic pyrazole CH$_3$ singlet signals resonating in the 2.50–2.60 ppm range in the NMR spectra.

3.1.2. Synthesis of 4-MeS-AAP-NF (**6a**)

The new visible-light-responsive phenylalanine-based low-molecular-weight gelator ligand was synthesized using the efficient DCC-mediated coupling reaction method as described in Scheme 2 below [38]. In this approach, the carboxylic acid functionalized precursor compound 4-MeS-AAP-CH$_2$CO$_2$H was reacted with NHS, followed by the addition of DCC. After completion of the reaction, the solvent was removed by rotary evaporation under reduced pressure and used without purification for further reactions. The resulting residue was dissolved in acetone and reacted with an aqueous solution of phenylalanine in the presence of sodium carbonate as a base. After removal of the solvent via rotary evaporation, the crude product was purified by silica gel column chromatography using dichloromethane/methanol solvent mixtures affording the desired photo-switchable phenylalanine conjugated 4-MeS-AAP-NF (**6a**) product as a bright orange to yellow solid with 81% yield and with good solubility in alkaline aqueous/methanol solution. In these studies, the arylazopyrazole moiety was conjugated with the phenylalanine amino acid due to its known propensity to form stable supramolecular gels [12,14]. The resulting 4-MeS-AAP-NF compound was characterized by ^{1}H-NMR, ^{13}C-NMR, electron spray mass spectroscopy (ESI-MS), and Fourier transform infrared (FTIR) spectroscopy. All the spectroscopy data were found to strongly support the purity and structure of the compound (see Figures S9, S10, S12 and S13).

Scheme 1. Synthetic route for 4-MeS-AAP-CH$_2$CO$_2$H (**5a**).

Scheme 2. Synthetic route for 4-MeS-AAP-NF (**6a**).

In the ^{1}H-NMR spectrum, the compound 4-MeS-AAP-NF displays four separate singlets for methylene protons (4.88 ppm), methyl protons of 4-methylthio (2.59 ppm), and the two methyl protons of the pyrazole ring (2.46–2.49 ppm). Apart from these signals, the ^{1}H-NMR spectrum of compound 4-MeS-AAP-NF show resonances at 7.17–760 ppm corresponding to the pyrazole ring and aromatic protons. In addition, in the ^{13}C-NMR spectrum of compound 4-MeS-AAP-NF, four well-separated resonances were observed for the methylene and methyl carbons of the pyrazole ring. The remaining ^{13}C-NMR signals show chemical shifts typical of the signals for the carbonyl carbon and in the aromatic region due to the phenyl rings of arylazopyrazole and phenylalanine moieties.

3.1.3. Gelation Study

To assess the gelation behavior of the phenylalanine-functionalized arylazopyrazole-based LMWG gelator ligand (4-MeS-AAP-NF), 20 mg of the 4-MeS-AAP-NF were placed in a glass vial and dissolved in a 9:1 alkaline methanol/water (MeOH/H$_2$O) solvent mixture at pH ~11.60. At this pH, a clear yellow solution of the 4-MeS-AAP-NF was formed. No gel formation was observed after sonication or vortex treatment of the clear alkaline solution of the 4-MeS-AAP-NF compound. Furthermore, lowering the pH of the solution followed by vortex treatment provided an orange–yellow suspension. These results indicate that the 4-MeS-AAP-NF alone has no gelation ability under both alkaline and acidic conditions. As shown in Scheme 2, the 4-MeS-AAP-NF ligand has N-pyrazole and O-carboxylic acid functionalities that can form coordination complexes with various metal ions, which could potentially affect the nature of self-assembly and gelation ability. Hence, to see whether the 4-MeS-AAP-NF form metallogels, we examined the self-assembly and gelation ability of the 4-MeS-AAP-NF in the presence of a series of divalent metal ions such as Ca^{2+}, Ni^{2+}, Cu^{2+}, Co^{2+}, and Zn^{2+} at room temperature (Figure 2). The gelation studies were carried out by mixing alkaline MeOH/H$_2$O solution of 4-MeS-AAP-NF ligand with aqueous metal salts in a 2:1 ligand-to-metal ratio upon sonication or by vortex treatment. While the 4-MeS-AAP-NF ligand by itself was unable to form a gel, the addition of different divalent metal ions resulted in the formation of a stable self-standing opaque orange matellogel after vortex or sonication treatment for 5 min, which was confirmed by the test tube inverting method (Figure 2). This indicates that the gel formation was triggered by metal ions. Next, the influence of anions was tested using ZnSO$_4$, Zn(NO$_3$)$_2$, and Zn(CH$_3$CO$_2$)$_2$ salts under alkaline (pH~11.6) conditions with a 2:1 ligand to Zn^{2+} mole ratio (Figure 2). The results of the experiment show that all anions led to the formation of stable metallogels, indicating that the gelation process was counterion-independent. The formed metallogels were stable, as no disruption of the gel was observed upon standing for several months at room temperature.
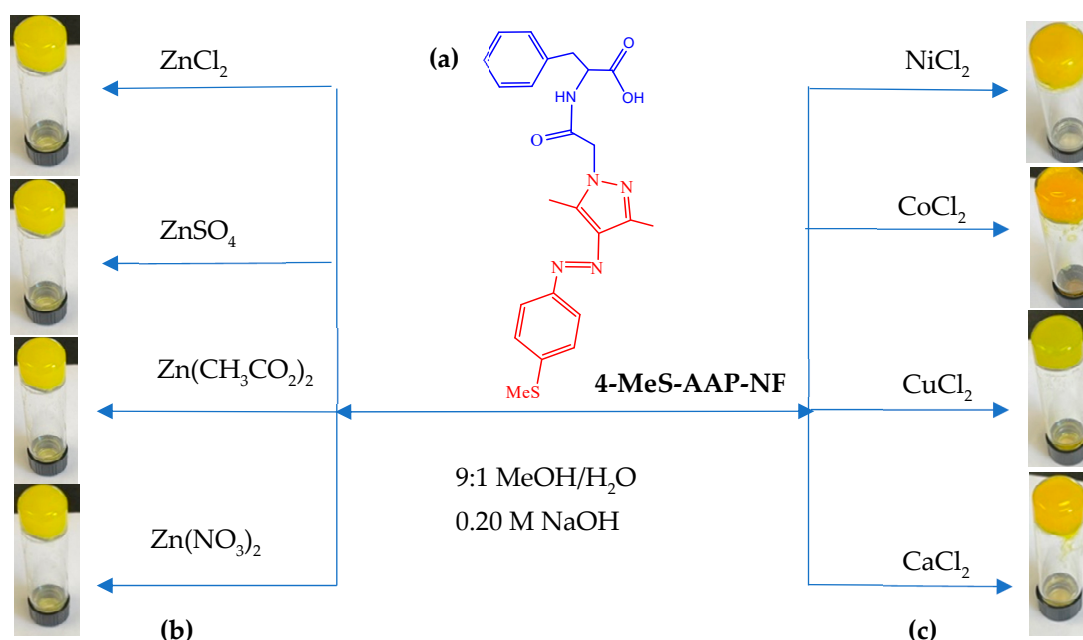

Figure 2. (**a**) Chemical structure of the 4-MeS-AAP-NF gelator; (**b**) pictures of glass vials containing the metallogel assembly formed by the metal ion triggered self-assembly; (**c**) picture of vials Zn^{2+} ion triggered self-assembly of metallogels.

3.1.4. Photoisomerization Properties of 4-MeS-AAP-NF

The photo-switching properties of the phenylalanine functionalized ligand (4-MeS-AAP-NF) were studied using UV-visible spectroscopy. The light-induced photo-switching

behavior of 4-MeS-AAP-NF is shown in Figure 3. Before light irradiation, the solution of 4-MeS-AAP-NF exhibited a strong absorption band at 335 nm corresponding to the π–π* transition of the *trans*-isomer of the 4-MeS-AAP-NF moiety, whereas the n-π* absorption peak appeared at 380 nm. After exposing the sample to blue light (λ = 405 nm), the strong absorption band at 335 nm corresponding to the π–π* transition was significantly reduced and blue-shifted, which is a normal characteristic of AAP-based molecular switches [15,25–29]. Similarly, a decrease in intensity of the absorbance around 384 nm due to the n–π* transition was also observed, which is the opposite of the usual increase seen for AAPs (Figure 3a). Next, exposure to green light (λ= 530 nm) results in the recovery of the initial absorption band for the *trans*-isomer, showing a strong absorption band with a maximum centered at 335 nm and a band at 384 nm (Figure 3b). This indicates a near-complete reversibility of the process under alternating blue and green light irradiation. The *cis:trans* ratio for the 4-MeS-AAP-NF ligand at the photostationary (PSS) state reached after 80 s blue light irradiation was found to be 85:15, as determined by UV-vis spectroscopy.
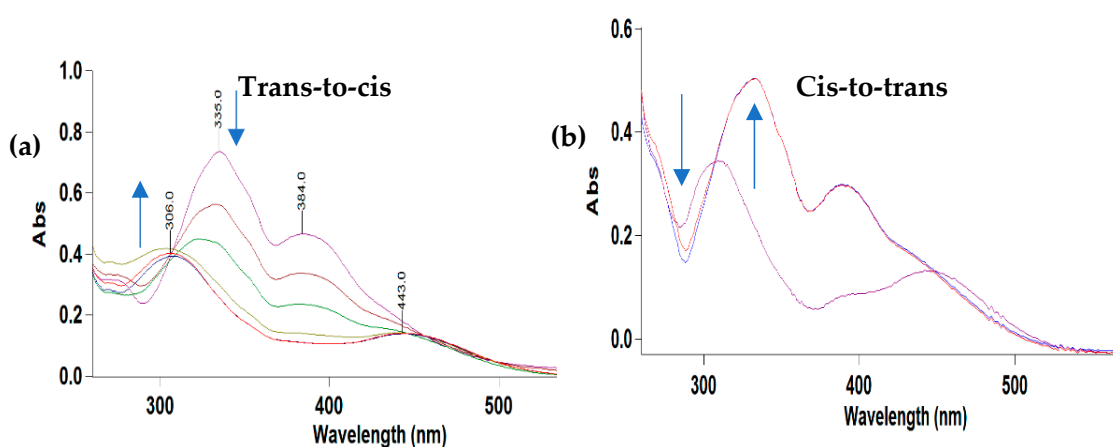

Figure 3. UV-vis absorption spectra of 4-MeS-AAP-NF: (**a**) trans-to-cis isomerization upon irradiation with blue (λ = 405 nm) 0–80 s. (**b**) Cis-to-trans isomerization upon irradiation with green light (λ = 530 nm) 0–80 s.

3.1.5. Light-Responsive Behavior of the Metallogels

The light-induced behavior of metallogel assemblies is influenced by the reversible *trans*-to-*cis* photoisomerization of the arylazopyrazole (AAP) molecules. Ravoo and co-workers recently reported photo-responsive gels based on tripodal low-molecular-weight gelators coupled with the AAP moiety. In their studies, they show that the gels undergo reversible sol–gel transitions due to the photoisomerization of the AAP unit in the LWG from the planar *trans*-isomer to the twisted *cis*-isomer. The authors also demonstrate that the AAP moiety present in the arms of the tripodal LMWGs contributes to the self-assembly process through the π–π interactions and was responsible for the reversible sol–gel transitions [27]. From these studies, we presumed that the phenylalanine-based 4-MeS-AAP-NF ligand that is coupled with the AAP moiety would serve as a good candidate for the fabrication of gels, in which the AAP unit would contribute to the supramolecular interactions through π–π stacking and provide photo-responsiveness. The photo-responsive behavior of the gels was studied using the Zn^{2+}-4-MeS-AAP-NF metallogel assembly as a representative example, as shown in Figure 4. The gel formed by the Zn^{2+}-4-MeS-AAP-NF assembly began to partially collapse upon irradiation with blue light (λ = 405 nm) and induced a gradual gel-to-sol transition (Figure 4b). The resulting partial collapse of the gel is due to the formation of the twisted cis-isomer upon irradiation with blue light (Figure 4a). The twisted *cis*-isomer disfavors self-assembly by preventing intermolecular interactions compared to the linear trans-isomer, which favors self-assembly [27]. As shown in Figure 4b, irradiation with green light at λ = 530 nm for 5 min followed by vortex treatment could revert the partially collapsed gel back into the original state, as confirmed by the inverted

vial test (Figure 4b). The partial collapse of the gel induced by light irradiation also resulted in a color change from yellow to orange, which could be attributed to the isomerization of the AAP moiety in the 4-MeS-AAP-NF ligand from the trans to the cis-isomer.
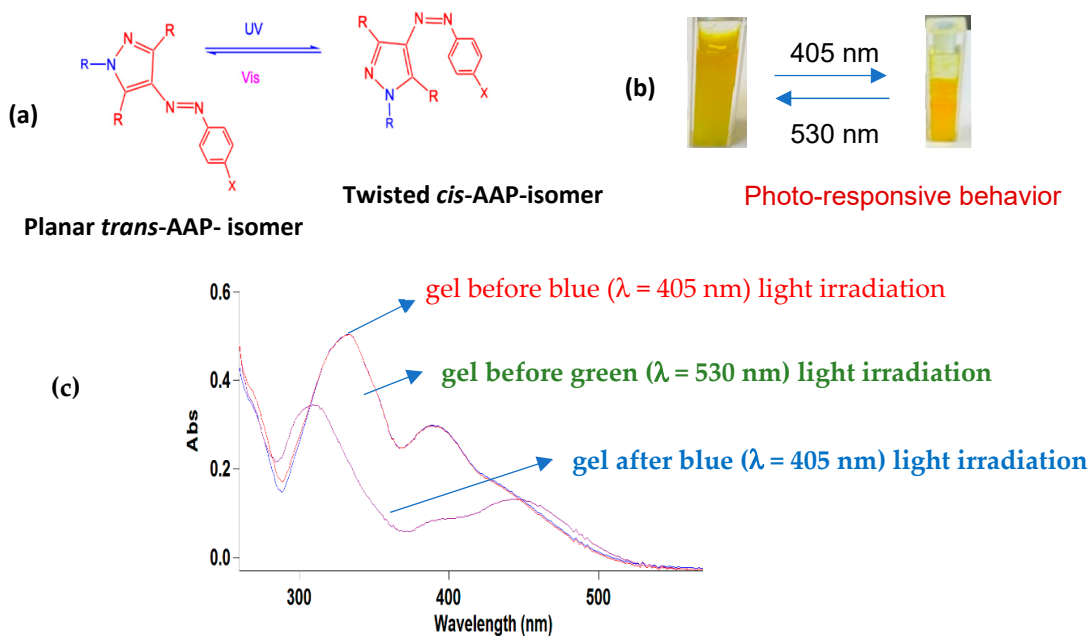

Figure 4. (**a**) Reversible light-induced conformation changes of the AAP moiety. (**b**) Photographic image of the reversible photo-induced gel-to-sol phase change in the gel formed by the Zn^{2+}-4-MeS-AAP-NF assembly upon alternating blue and green light irradiation; (**c**) changes in the UV-Vis spectrum of DMSO solutions of the Zn^{2+}-4-MeS-AAP-NF gel upon treating with blue light $\lambda = 405$ nm and recovery of the spectrum after green light $\lambda = 530$ nm irradiation.

The light-induced sol–gel transition can also be monitored by following the characteristic peaks of the trans-isomer during both blue light irradiation and subsequent green light exposure. The UV-vis spectral change investigations were carried out using a DMSO solution of the Zn^{2+}-MeS-AAP-NF gel. As described in Figure 4c, the Zn^{2+}-MeS-AAP-NF gel assembly displays excellent forward and reverse photoisomerization behavior upon alternating blue and green light irradiations, respectively. These results demonstrate the remarkable advantages offered by the emerging AAP photoswitches as the free MeS-AAP-NF ligand and the Zn^{2+}-MeS-AAP-NF assembly exhibit excellent light-induced *trans*-to-*cis* isomerization. The excellent photo-switchability of the AAP unit in the metallogel assembly is confirmed by the near quantitative (~100%) conversion efficiency of the *cis*-Zn^{2+}-4-MeS-AAP-NF to the *trans* isomer at the photo stationary state within (5 min) estimated based on the UV-vis spectra.

The M^{2+}-MeS-AAP-NF (M^{2+} = Ca^{2+}, Co^{2+}, Cu^{2+}, Ni^{2+}) gels exhibit similar spectral changes to that of Zn^{2+}-MeS-AAP-NF (as the UV-vis data for these is remarkably similar to that of the Zn^{2+} it is not given). These results indicate that the gel-to-sol phase transition does not depend on the type of divalent metal ions used.

4. Scanning Electron Microscopy (SEM) Study

To further investigate the morphological features of the metallogel self-assembly obtained from 4-MeS-AAP-NF and different divalent metal ions, scanning electron microscopy (SEM) images of the gels were recorded. Figure 5 shows SEM images of the different metallogels.
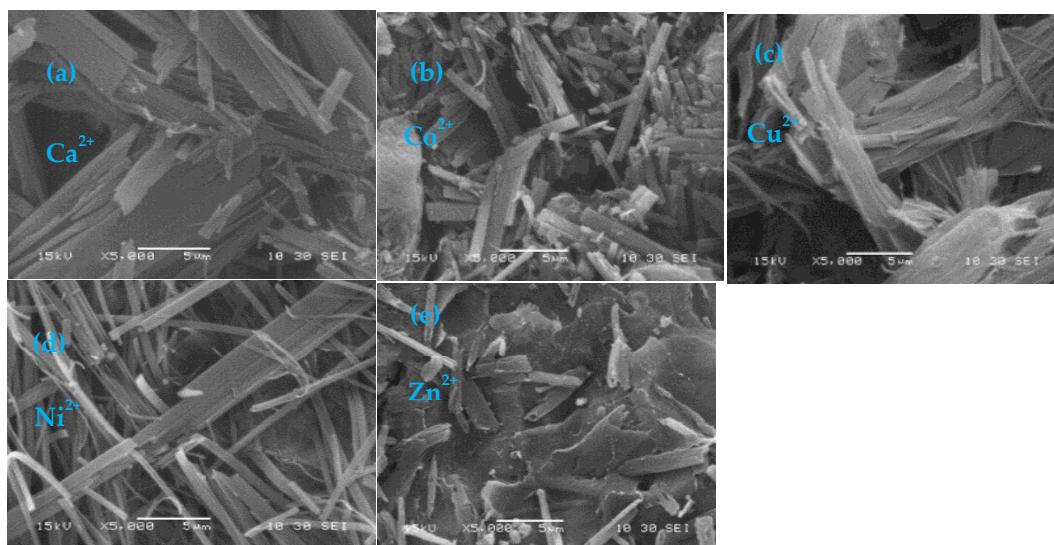
Figure 5. SEM images of metallogels obtained from (**a**) Ni^{2+}- 4-MeS-AAP-NF, (**b**) Ca^{2+}-4-MeS-AAP-NF, (**c**) Cu^{2+}-4-MeS-AAP-NF, (**d**) Co^{2+}-4-MeS-AAP-NF, and (**e**) Zn^{2+}-4-MeS-AAP-NF in alkaline solution of pH~11:60.

The SEM images revealed that the M^{2+}-MeS-AAP-NF (M^{2+} = Ni^{2+}, Cu^{2+}, Co^{2+}, Ca^{2+}, Zn^{2+}) xerogel form distinct morphologies depending on the type of metal ions used. The images clearly show that the Ca^{2+}-containing gels showed a plate-like structure, while the Co^{2+} gels display dense rod-like morphology (Figure 5a,b). Meanwhile, the Cu^{2+} and Ni^{2+}-based metallogels form intertwined nanofibrillar network structures (Figure 5c,d), whereas Zn^{2+} shows a dense sheet-like structure (Figure 5e). This suggests that the different divalent metal ions coordinated with the 4-MeS-AAP-NF gelator lead to varied morphology. These images also clearly revealed the influence of metal ions in gel morphology in the arylazopyrazole functionalized phenylalanine-based metallogels.

To check whether there was any effect of anions on the morphology of the gels, SEM experiments were also performed for different zinc salts, including $ZnCl_2$, Zn $(NO_3)_2$, $Zn(CH_3CO_2)_2$, and $ZnSO_4$. From the SEM images (Figure S11), it was found that CH_3COO^- based gels form nonuniform plate-like structures, and NO_3^- gels show densely intertwined nanofibers, whereas SO_4^{2-} form a laminal-type morphology. These results demonstrate that the morphology of the gels was dependent on the counter anions of the zinc salts.

5. Rheological Study

To examine the viscoelastic properties of the metallogel assemblies, rheological studies were performed using freshly prepared samples at room temperature. The dynamic amplitude sweeps rheological experiments conducted on all the metallogels assemblies showed that the storage modulus (G′) is significantly higher than their loss modulus (G″), indicating that the gels are elastic rather than viscous materials (Figure 6). Comparative changes in the G′/G″ values clearly show that the metallogels fabricated using Cu^{2+} display the strongest viscoelastic character in these series, while Ca^{2+} showed the lowest value. The storage modulus (G′) of the metallogels values follow the mechanical strength order: $Cu^{2+} > Ni^{2+} > Co^{2+} > Zn^{2+} > Ca^{2+}$. This trend in the mechanical strength of the metallogel is driven by the stability of metal ion complex formation and fits well with the Irving–Williams series [3,39,40]. Overall, the results of the rheological experiments (i.e., G′ > G″) confirm the mechanical stability and viscoelastic nature of the gels.
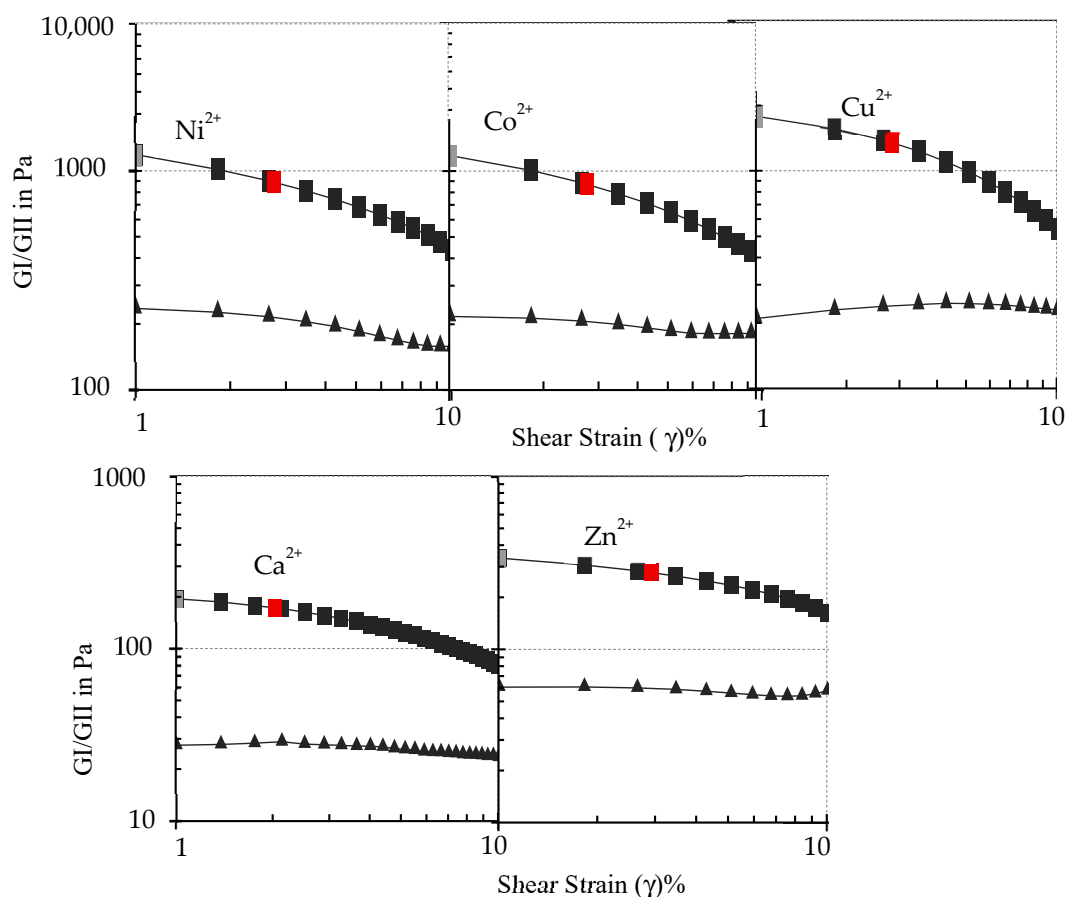
Figure 6. Dynamic strain amplitude rheological experiment for the M^{2+}-4-MeS-AAP-NF gels.

6. Fourier Transform Infrared Spectroscopy (FT-IR) Studies

Fourier transform infrared (FT-IR) spectroscopy was conducted to probe the nature of the interactions and the probable coordination modes between the 4-MeS-AAP-NF ligand and the divalent metal ions. As representative examples, the FT-IR spectrum of the pure 4-MeS-AAP-NF ligand and the M^{2+}-4-MeS-AAP-NF (M = Ca^{2+}, Co^{2+}) metallogels are provided in (Figure 7). In the non-gel state, the 4-MeS-AAP-NF ligand displayed peaks at 3298 cm^{-1}, 1558 ccm^{-1} corresponding to N-H stretching and bending vibration modes, and 3056 cm^{-1}, 1718 cm^{-1} for the carboxylic acid (-COOH) group. The amide (-C=O) stretching band appeared at 1670 cm^{-1}.

However, in the M^{2+}-4-MeS-AAP-NF metallogel state, the vibrational bands of the carboxylic acid group at 3056 cm^{-1} and 1718 cm^{-1} disappeared. The absence of these bands in the metallogel state indicates the participation of the carboxylate groups in the coordination of the metal ions in the gel [15,41–43]. Moreover, the peak at 3298 cm^{-1} (-N-H) in the non-gel state is shifted to 3325 cm^{-1} for Ca^{2+} and 3321 cm^{-1} for Co^{2+} in the metallogels suggesting participation of the N-atom of the amide unit in the metal ion coordination. The N-H bending band has also been shifted from 1558 cm^{-1} to 1580 cm^{-1} for Ca^{2+} and 1569 cm^{-1} for Co^{2+} in the metallogel state. Similarly, the amide (-C=O) stretching band at 1670 cm^{-1} is shifted to 1625 cm^{-1} for Ca^{2+} and 1621 cm^{-1} for Co^{2+}. The decrease in the -C=O stretching frequency and broadening of the N-H stretching band, coupled with the increase in the N-H bending mode in the metallogels suggests the formation of hydrogen bonding networks during the gelation process. Furthermore, the stretching vibrations of the C=N bond at 1420 cm^{-1} in the pyrazole ring are shifted and split into two peaks (1435 cm^{-1} and 1394 cm^{-1}) for Ca^{2+} and (1433 cm^{-1} and 1397 cm^{-1}) for Co^{2+}, suggesting coordination of the N-atom of the pyrazole ring in the metallogels [42]. The FTIR spectra of the Cu^{2+}, Ni^{2+}, and Zn^{2+}-based metallogels display similar behavior with

the (-COOH), N-H, and -C=O carboxylate and amide functionalities to those of Ca^{2+} and Co^{2+}. The -C=N stretching of the pyrazole ring also shows similar vibrational frequencies (Figure S12) in the Supplementary Materials.
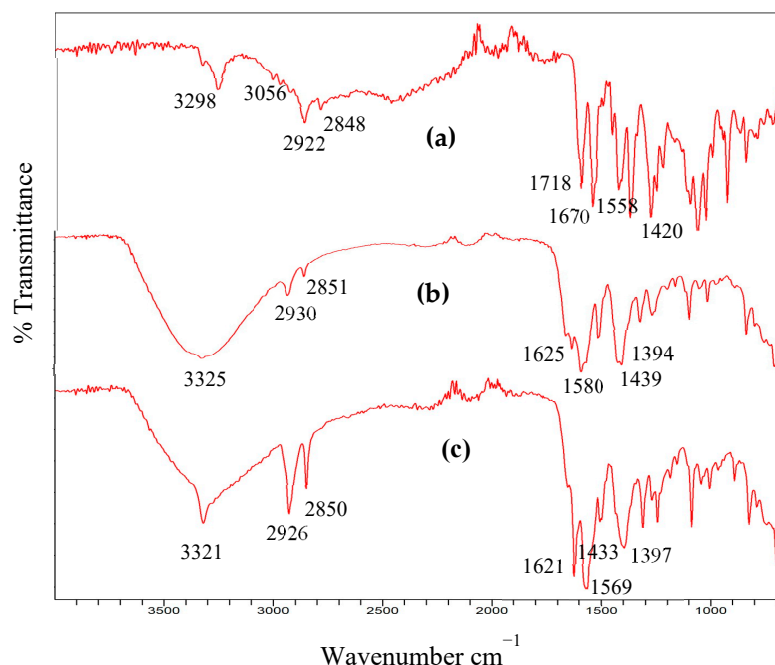

Figure 7. FTIR spectra of (a) AAP-NF, (b) Ca^{2+}-AAP-NF, and (c) Co^{2+}-AAP-NF xerogels.

7. Mass Spectra (ESI-MS) Studies

To gain structural insights into the presence of metal ions for the ligand, we obtained electron spray mass spectra (ESI-MS) of the free ligand and the metallogels (Figures S13–S17). In the ESI-MS spectra, the free 4-MeS-AAP-NF ligand displays the parent molecular ion peak of $[4\text{-MeS-AAP-NF} + H]^+$ (Figure S13). Spraying dilute methanol solutions of the xerogels obtained from 4-MeS-AAP-NF + Ca^{2+}, 4-MeS-AAP-NF + Co^{2+}, and 4-MeS-AAP-NF + Ni^{2+} gelator ligand resulted in the formation of a prominent ion peak signal corresponding to $[(4\text{-MeS-AAP-NF})M\text{-Cl}]^+$ (M = Ca^{2+}, Co^{2+}, Ni^{2+}) (Figures S14–S16), suggesting the formation of a mononuclear tetrahedral environment around the metal ion. On the other hand, the addition of a Cu^{2+} metal ion caused dimerization, as evident from the ESI-MS molecular ion peak, $[(4\text{-MeS-AAP-NF})_2Cu + K]^+$ (Figure S17). However, no clean ESI-MS was detected for the Zn^{2+}-based metallogels. As described in the experimental section, stable self-standing metallogels were formed using a 2:1 ligand-to-metal ratio. However, analysis of the MS-ESI study of the xerogels formed by the different metal ions suggested a 1:1 ratio, which was identified by the formation of an ionized form of the M^{2+}-4-MeS-AAP-NF complex, $[(4\text{-MeS-AAP-NF})M]^+$ (M = Ca^{2+}, Co^{2+}, Ni^{2+}) (Figures S14–S16). These results strongly suggest that the 4-MeS-AAP-NF likely acts as a tridentate ligand, which binds to M^{2+} and forms a tetra-coordination compound of M^{2+}-4-MeS-AAP-NF with the fourth coordination site probably occupied by a choro ligand. The addition of different metal ions into the alkaline aqueous solution of the M^{2+}-4-MeS-AAP-NF gelator can induce the formation of metal coordination complexes, which may first self-assemble into fibers and re-assemble the fibers further into hierarchical intertwined nanofibrillar network structures probably arising from the synergistic effects of metal–ion complexation and through various non-covalent interactions that include H-bonding interactions and π–π stacking interactions.

8. Conclusions

In summary, we have described the preparation of a simple phenylalanine conjugated visible-light-responsive arylazopyrazole-based low-molecular-weight gelator ligand that readily forms stable metallogels by mixing with different divalent metal ions. The metallogels are constructed by mixing an alkaline aqueous methanol/water solution of an arylazopyrazole substituted phenylalanine derivative gelator ligand (4-MeS-AAP-NF) with aqueous solutions of divalent metal salts. We found that the 4-MeS-AAP-NF gelator can form stable metallogels in the presence of various divalent metal ions and self-assemble into nanofibers with different morphologies. However, the 4-MeS-AAP-NF alone in alkaline or acidic conditions does not form any gel. This observation indicates that the gelation process is triggered by the divalent metal ions. The results also showed that the gel formation is not specific to any metal ions. The excellent photo-switching behavior of the AAP moiety was preserved in the metallogel assembly, enabling the formation of photo-responsive gels that display light-triggered phase transition, which can be partially reversed by alternating blue and green light irradiation. The gel-to-sol phase transition of the metallogels was also found to be independent of the type of metal ions used. The ESI-MS and FTIR studies suggest that tetrahedral coordination complexes are formed, followed by hierarchical self-assembly into a modified supramolecular gel. This work provides some inspiration for the convenient fabrication of a new class of visible light-responsive self-assembled soft materials that combine metal-specific properties and light.

Supplementary Materials: The following supporting information can be downloaded at: https://www.mdpi.com/article/10.3390/photochem3040026/s1. Supporting information is given for ^{1}H-NMR, ^{13}C-NMR, ESI-MS, FT-IR, and Rheology; Figure S1: ^{1}H-NMR spectrum of compound **2a** in CDCl$_3$; Figure S2: ^{13}C-NMR spectrum of compound **2a** in CDCl$_3$; Figure S3: ^{1}H-NMR spectrum of compound **3a** in CDCl$_3$; Figure S4: ^{13}C-NMR spectrum of compound **3a** in CDCl$_3$; Figure S5: ^{1}H-NMR spectrum of compound **4a** in CDCl$_3$; Figure S6: ^{13}C-NMR spectrum of compound **4a** in CDCl$_3$; Figure S7: ^{1}H-NMR spectrum of compound 4-MeS-AAP-CH$_2$CO$_2$H (**5a**) in DMSO; Figure S8: ^{13}C-NMR spectrum of compound 4-MeS-AAP-CH$_2$CO$_2$H (**5a**) in DMSO; Figure S9: ^{1}H-NMR spectrum of compound 4-MeS-AAP-NF (**6a**) in DMSO; Figure S10: ^{13}C-NMR spectrum of compound 4-MeS-AAP-NF (**6a**) in DMSO; Figure S11: dynamic strain amplitude rheological experiment for different anions of the Zn^{2+}-4-MeS-AAP-NF metallogels; Figure S12: FTIR spectra of (a) 4-MeS-AAP-NF; (b) Cu^{2+}-4-MeS-AAP-NF; (c) Ni^{2+}-4-MeS-AAP-NF and (d) Ni^{2+}-4-MeS-AAP-NF xerogels; Figure S13: ESI-MS spectrum of compound 4-MeS-AAP-NF (**6a**); Figure S14: ESI-MS spectrum of compound Ca^{2+}+4-MeS-AAP-NF metallogel; Figure S15: ESI-MS spectrum of compound Co^{2+}+4-MeS-AAP-NF metallogel; Figure S16: ESI-MS spectrum of compound Ni^{2+}+4-MeS-AAP-NF metallogel; Figure S17: ESI-MS spectrum of compound Cu^{2+}+4-MeS-AAP-NF metallogel.

Conflicts of Interest: The authors declare no conflict of interest.

References

1. Nakajima, K.; Hauser, H.; Li, T.; Pfeifer, R. Exploiting the Dynamics of Soft Materials for Machine Learning. *Soft Robot.* **2018**, *5*, 339–347. [CrossRef]
2. Loos, J.N.; Boott, C.E.; Hayward, D.W.; Hum, G.; MacLachlan, M.J. Exploring the Tunable Optical and Mechanical Properties of Multicomponent Low-Molecular-Weight Gelators. *Langmuir* **2021**, *37*, 105–114. [CrossRef]

3. Basak, S.; Singh, I.; Kraatz, H.-B. Ion-Dependent Modulation of Self-Healing Hydrogels. *ChemistrySelect* **2017**, *2*, 451–457. [CrossRef]

4. Biswas, P.; Ganguly, S.; Dastidar, P. Stimuli-Responsive Metallogels for Synthesizing Ag Nanoparticles and Sensing Hazardous Gase. *Chem. Asian J.* **2018**, *13*, 1941–1949. [CrossRef]

5. Malviya, N.; Sonkar, C.; Ganguly, R.; Mukhopadhyay, S. Cobalt Metallogel Interface for Selectively Sensing L-Tryptophan among Essential Amino Acids. *Inorg. Chem.* **2019**, *58*, 7324–7334. [CrossRef]

6. Canrinus, T.R.; Lee, W.W.Y.; Feringa, B.L.; Bell, S.E.; Browne, W.R. Supramolecular Low-Molecular-Weight Hydrogelator Stabilization of SERS-Active Aggregated Nanoparticles for Solution and Gas Sensing. *Langmuir* **2017**, *33*, 8805–8812. [CrossRef] [PubMed]

7. Jiang, Z.; Tan, M.L.; Taheri, M.; Yan, Q.; Tsuzuki, T.; Gardiner, M.G.; Diggle, B.; Connal, L.A. Strong, Self-Healable, and Recyclable Visible-Light-Responsive Hydrogel Actuators. *Angew. Chem.* **2020**, *132*, 7115–7122. [CrossRef]

8. Giammanco, G.E.; Sosnofsky, C.T.; Ostrowski, A.D. Light-Responsive Iron(III)-Polysaccharide Coordination Hydrogels Controlled Delivery. *ACS Appl. Mater. Interfaces* **2015**, *7*, 3068–3076. [CrossRef]

9. Archer, J.; Pianowski, Z.L.; Karcher, J.; Schneider, K. Photoresponsive self-healing supramolecular hydrogels for light-induced release of DNA and doxorubicin. *Chem. Commun.* **2016**, *52*, 3143–3146. [CrossRef]

10. Tao, M.; Xu, K.; He, S.; Li, H.; Zhang, L.; Luo, X.; Zhong, W. Zin-ion-Mediated Self-Assembly of Forky Peptides for Prostate Cancer-Specific Drug Delivery. *Chem. Commun.* **2018**, *54*, 4673–4676. [CrossRef] [PubMed]

11. Zhang, J.; Liu, S.; Li, H.; Tian, X.; Li, X. Tryptophan-Based Self-Assembling Peptides with Bacterial Flocculation and Antimicrobial Properties. *Langmuir* **2020**, *36*, 11316–11323. [CrossRef]

12. Das, T.; Häring, M.; Haldar, D.; Díaz, D.D. Phenylalanine and derivatives as versatile low-molecular-weight gelators: Design, structure and tailored function. *Biomater. Sci.* **2018**, *6*, 38–59. [CrossRef] [PubMed]

13. Shao, T.; Falcone, N.; Kraatz, H.-B. Supramolecular Peptide Gels: Influencing Properties by Metal Ion Coordination and Their Wide-Ranging Applications. *ACS Omega* **2020**, *5*, 1312–1317. [CrossRef] [PubMed]

14. Ghrayeb, M.; Chai, L. Demonstrating Principles Aspects of Peptide-and Protein-Based Hydrogels Using Metallogels Examples. *Isr. J. Chem.* **2022**, *62*, e202200011. [CrossRef]

15. Sallee, A.; Ghebreyessus, K. Photoresponsive Zn^{2+}-specific metallohydrogels coassembled from imidazole containing phenylalanine and arylazopyrazole derivatives. *Dalton Trans.* **2020**, *49*, 10441–10451. [CrossRef]

16. Li, Y.; Wei, C.-W.; Wang, X.-J.; Gao, S.-Q.; Lin, Y.-W. Amino Acid Derivative-based Ln-Metallohydrogels with Multi-Stimuli-Responsiveness and Applications. *Mol. Biomol. Spectrosc.* **2022**, *271*, 120901. [CrossRef]

17. Li, J.; Li, W.; Xia, D.; Xiang, C.; Chen, Y.; Li, G. Dynamic Coordination of Natural Amino Acids-Lanthanides to Control Reversible Luminescent Switching of Hybrid Hydrogels and Anti-Counterfeiting. *Dye. Pigm.* **2019**, *166*, 375–380. [CrossRef]

18. Gayen, K.; Basu, K.; Bairagi, D.; Castelletto, V.; Hamley, I.W.; Banerjee, A. Amino-Acid-Based Metallo-Hydrogel That Acts Like an Esterase. *ACS Appl. Bio Mater.* **2018**, *1*, 1717–1724. [CrossRef]

19. Liu, Z.; Zhao, X.; Chu, Q.; Feng, Y. Recent Advances in Stimuli-Responsive Metallogels. *Molecules* **2023**, *28*, 2274. [CrossRef]

20. Basak, S.; Nanda, J.; Banerjee, A. Multi-stimuli Responsive Self-healing Metallo-Hydrogels: Tuning of the Gel Recovery Property. *Chem. Commun.* **2014**, *50*, 2356–2359. [CrossRef]

21. de Luna, M.S.; Marturano, V.; Manganelli, M.; Santillo, C.; Ambrogi, V.; Filippone, G.; Cerruti, P. Light-responsive and self-healing behavior of azobenzene-based supramolecular hydrogels. *J. Colloid Sci.* **2020**, *568*, 16–24. [CrossRef] [PubMed]

22. Bindu, H.; Palanisamy, A. Polyethylene-Glycol-Based Thermoreversible Biscarbamate Hydrogels and Metallogels Synthesized through Non-Isocyanate Route. *ChemistrySelect* **2019**, *4*, 11052–11060. [CrossRef]

23. Dawn, A.; Pajoubpong, J.; Mesmer, A.; Mirzamani, M.; He, L.; Kumari, H. Manipulating Assemblies in Metallosupramolecular Gels, Driven by Isomeric Ligands, Metal Coordination, and Adaptive Binary Gelator Systems. *Langmuir* **2022**, *38*, 1705–1715. [CrossRef] [PubMed]

24. Xiong, W.; Zhou, H.; Zhang, C.; Lu, H. An Amino Acid-Based Gelator for Injectable and Multi-Responsive Hydrogel. *Chin. Chem. Lett.* **2017**, *28*, 2125–2128. [CrossRef]

25. Weston, C.E.; Richardson, R.D.; Haycock, P.R.; White, A.J.P.; Fuchter, M.J. Arylazopyrazoles: Azoheteroarene Photoswitches Offering Quantitative Isomerization and Long Thermal Half-Lives. *J. Am. Chem. Soc.* **2014**, *136*, 11878–11881. [CrossRef]

26. Gibson, R.S.L.; Calbo, J.; Fuchter, M.J. Chemical Z-E isomer switching of arylazopyrazols using acid. *ChemPhotoChem* **2019**, *3*, 372–377. [CrossRef]

27. Chu, C.-W.; Stricker, L.; Kirse, T.M.; Hayduk, M.; Ravoo, B.J. Light-responsive arylazopyrazolegelator: From organic to aqueous media and from supramolecular to dynamic covalent chemistry. *Chem. Eur. J.* **2019**, *25*, 6131–6140. [CrossRef]

28. Bhunia, S.; Dolai, A.; Samanta, S. c. *Chem. Commun.* **2020**, *56*, 10247–10250. [CrossRef]

29. Bhunia, S.; Dolai, A.; Bera, S.; Samanta, S. Near-Complete Bidirectional Photoisomerization of *para*-Dialkylamino-Substituted Arylazopyrazoles under Violet and Green or Red Lights. *J. Org. Chem.* **2022**, *87*, 4449–4454. [CrossRef]

30. Chu, C.-W.; Ravoo, B.J. Hierarchical supramolecular hydrogels: Self-assembly by peptides and photo-controlled release via host-guest interaction. *Chem. Commun.* **2017**, *53*, 12450–12453. [CrossRef]

31. Schnurbus, M.; Stricker, L.; Bart Jan Ravoo, B.J.; Braunschweig, B. Smart Air−Water Interfaces with Arylazopyrazole Surfactants and Their Role in Photoresponsive Aqueous Foam. *Langmuir* **2018**, *34*, 6028–6035. [CrossRef] [PubMed]

32. Lamping, S.; Stricker, L.; Bart Jan Ravoo, B.J. Responsive surface adhesion based on host–guest interaction of polymer brushes with cyclodextrins and arylazopyrazoles. *Polym. Chem.* **2019**, *10*, 683–690. [CrossRef]

33. Adam, V.; Prusty, D.K.; Centola, M.; Škugor, M.; Hannam, J.S.; Valero, J.; Bernhard Klockner, B.; Famulok, M. Expanding the Toolbox of Photoswitches for DNA Nanotechnology Using Arylazopyrazoles. *Chem. Eur. J.* **2018**, *24*, 1062–1066. [CrossRef] [PubMed]

34. Ghebreyessus, K.; Cooper, S.M., Jr. Photoswitchable Arylazopyrazole-Based Ruthenium(II)-Arene Complexes. *Organometallics* **2017**, *36*, 3360–3370. [CrossRef]

35. Kumar, N.; Masanori, J.; Wada, F.A. Polarity Controlled Reaction Path and Kinetics of Thermal Cis-to-Trans Isomerization of 4-Aminoazobenzene. *J. Phys. Chem. B* **2014**, *118*, 1891–1899. [CrossRef]

36. Peng, S.; Guo, Q.; Hartley, P.G.; Hughes, T.C. Azobenzene Moiety Variation Directing Self-Assembly and Photoresponsive Behavior of Azo-Surfactants. *J. Mater. Chem. C* **2014**, *2*, 8303–8312. [CrossRef]

37. Angelini, G.; Canilho, N.; Emo, M.; Kingsley, M.; Gasbarri, C. Role of Solvent and Effect of Substituent on Azobenzene Isomerization by Using Room-Temperature Ionic Liquids as Reaction Media. *J. Org. Chem.* **2015**, *80*, 7430–7434. [CrossRef]

38. Simon, T.; Wu, C.-S.; Liang, J.-C.; Cheng, C.; Ko, F.-H. Facile Synthesis of a Biocompatible Silver Nanoparticle Derived Tripeptide Supramolecular Hydrogel for Antibacterial Would Dressing. *New J. Chem.* **2016**, *40*, 2036–2045. [CrossRef]

39. Shriver, D.F.; Atkins, P.; Langford, C.H. *Inorganic Chemistry*, 2nd ed.; W. H. Freeman and Co.: New York, NY, USA, 1997.

40. Stendahl, J.C.; Rao, M.S.; Guler, M.O.; Stupp, S.I. Intermolecular Forces in the Self-Assembly of Peptide Amphiphile Nanofibers. *Adv. Funct. Mater.* **2006**, *16*, 499–508. [CrossRef]

41. Ray, S.; Das, A.K.; Banerjee, A. pH-Responsive, Bolaamphiphile-Based Smart Metallo-Hydrogels as Potential Dye-Adsorbing Agents, Water Purifier, and Vitamin B_{12} Carrier. *Chem. Mater.* **2007**, *19*, 1633–1639. [CrossRef]

42. Wei, C.W.; Wang, X.J.; Gao, S.Q.; Wen, G.B.; Lin, Y.W. A Phenylalanine Derivative Containing a 4-Pyridine Group Can Construct Both Single Crystals and a Selective Cu-Ag Bimetallohydrogel. *Eur. J. Inorg. Chem.* **2019**, *2019*, 1349–1353. [CrossRef]

43. Wei, C.W.; Wang, X.J.; Gao, S.Q.; Wen, G.B.; Lin, Y.W. A La $^{3+}$-selective metallohydrogel with a facile gelator of a phenylalanine derivative containing an imidazole group. *Dalton Trans.* **2018**, *47*, 13788–13791. [CrossRef] [PubMed]